

## Article

# A Realistic Spark-Gap Model in Computer Simulation of Blumlein Transmission Line

Bartosz Chaber \* and Wiktor Łodyga 

Department of Electrical Engineering, Warsaw University of Technology, 00-661 Warsaw, Poland; wiktlor.lodyga.dokt@pw.edu.pl

\* Correspondence: bartosz.chaber@pw.edu.pl

**Abstract:** Over the years, the use of numerical simulations in the development of high voltage pulse generators has become a standard approach. Nevertheless, the modeling of spark-gaps, one of the most commonly used switching devices in such generators, has always been a weak point of the process, especially in coupled circuit and field simulations. Although the complex SPICE spark-gap models do exist, it is difficult or impossible to directly couple them with field simulations. Thus, in many cases, the spark-gap models used were elementary and required many assumptions, which led to the prolongation of the design process. Our paper describes the coupling of a realistic circuit model of an air spark-gap, with a Finite Element Method simulation, solving the wave equation in the time domain. The simulation describes the operation of a Blumlein transmission line as a pulse generator. One of the advantages of the proposed solution is that the input parameters of the empirical model are measurable physical quantities characterizing the spark-gap circuit. We have carried out two numerical experiments testing the simulation for both the matched, resistive load and for a dipole antenna connected to the output of the Blumlein transmission line. The test results confirm that the circuit-field simulation can model Blumlein transmission lines with both simple elements (e.g., resistors) and complex circuits (e.g., an equivalent circuit of a dipole antenna) attached to its terminals.

**Keywords:** finite element method; circuit simulation; high voltage engineering; pulsed power generation



**Citation:** Chaber, B.; Łodyga, W. A Realistic Spark-Gap Model in Computer Simulation of Blumlein Transmission Line. *Energies* **2022**, *15*, 3919. <https://doi.org/10.3390/en15113919>

Academic Editor: Tek Tjing Lie

Received: 26 April 2022

Accepted: 24 May 2022

Published: 26 May 2022

**Publisher's Note:** MDPI stays neutral with regard to jurisdictional claims in published maps and institutional affiliations.



**Copyright:** © 2022 by the authors. Licensee MDPI, Basel, Switzerland. This article is an open access article distributed under the terms and conditions of the Creative Commons Attribution (CC BY) license (<https://creativecommons.org/licenses/by/4.0/>).

## 1. Introduction

Our work aims at coupling an empirical circuit model of a spark-gap with an electromagnetic field simulation. This paper presents a computer simulation using a two-dimensional, transient, circuit-field model of a Blumlein transmission line with two different devices connected as its load. This hybrid model could aid in designing more efficient pulsed power generators by better capturing the effects of spark-gap characteristics.

The majority of high, pulsed power generators are coupled with transmission lines in order to propagate the generated high voltage pulses through them. One of the greatest challenges of developing such systems is to minimize impedance mismatches, which cause reflections, significantly lowering the overall efficiency of generators. Very often, field simulations of wave propagation are used to resolve this issue. Moreover, many high voltage generators use spark-gaps as their switching devices that can dynamically reconfigure the topology of different pulse generators (e.g., Marx generator, Blumlein pulse forming line, switched wave oscillators, etc.). Modelling the switching process of spark-gaps is not easy. Spark-gaps cannot switch between their on and off states instantaneously. The switching process is controlled by the physics of the microscopic reactions in the plasma created due to the ionization of dielectric gas in a spark-gap. Spark-gaps are often incorporated into simulations as lumped elements, e.g., as a time-varying resistor. The function describing the change of resistance affects the basic parameters of the output, i.e.,

the rise time of the voltage pulse. Sometimes an additional inductor is used to represent the inductive character of the conducting spark channel.

The simplest spark-gap circuit switches at a given time by way of a smooth transition between the high and low resistance values within a defined time range. This approach neglects the actual breakdown voltage values and geometry of the actual spark-gap. One could also implement the switch as a nonlinear element similar to the SPICE model by Basso [1], using Zener diodes. However, it does not try to capture some of the underlying aspects of the electrical discharge evolution, i.e., variable resistance and inductance of the conducting channel. There are models which try to use empirical models of arc resistance based on the changing discharge channel radius. A circuit model introduced by [2] also takes into account the time-varying inductance of the arc (due to the changing channel's radius). In [3], a constant channel radius and constant inductance have been assumed.

Approaches were made at building a plasma model of a spark-gap, which is a great undertaking given the complexity of the process of forming a discharge channel in gases. In [4] the initial channel radius was based on the averaged width of the ionization avalanche simulated with a kinetic model of argon and neon gases. Although the use of the kinetic description of plasma evolution needs relatively few assumptions on the numerical model, they are much more computationally intensive.

It has to be noted that there were successful approaches that have incorporated the basic spark-gap model in the process of designing high voltage pulse generators [5] based on an electromagnetic field simulation. They have proven that with correct assumptions regarding the operation of spark-gaps in the system, a rather basic (in this case Basso's) model was able to help in designing an efficient pulse generator. On the other hand, the use of a more realistic model allowed us to reasonably match experimental voltage waveforms from a physical Marx generator [6]. It is important to say that, despite using a more sophisticated model, there were still interesting effects in the measured voltage pulses that were not represented by the circuit model. To the best of our knowledge, the model [6] has not yet been coupled with a Finite Element Method time-domain electromagnetic field solver.

Nevertheless, it is useful to have a circuit model of spark-gap switching devices that relies on relatively few assumptions regarding its parameters. With use of the coupling method presented in this paper, it should also be possible to substitute the model of the high voltage switch with an even more realistic model based on even fewer assumptions. The main objective of our research is to test if coupling and electromagnetic field simulation with a realistic spark-gap circuit model allow the representation of the nonlinear effects of the electrical discharge in the Blumlein transmission line. We will also test which assumptions on the parameters and operation of spark-gaps can be dropped with the new model (i.e., can the time of electrical breakdown be determined by the model or does it have to be prescribed?).

## 2. Spark-Gap Circuit Model

SPICE circuit simulators solving electrical circuits, with Modified Nodal Analysis, are well known and have attracted significant attention over the last fifty years. They are also extensible in the sense that they allow the creation of additional models by using other circuit elements, e.g., behavioral sources. However, an interesting alternative method has been presented in [7] and implemented in the project ACME.jl [8]. It allows the defining of nonlinear circuit elements using the Julia programming language [9]. Nonlinearity of circuit elements is defined with equation  $f(\mathbf{q}) = 0$ , where  $\mathbf{q}$  is a vector of nonlinear state variables for the element. A nonlinear equation is associated with each nonlinear element and is assembled by ACME.jl into a Jacobian matrix for solving the nonlinear circuit.

Although there are attempts at modeling high-voltage switches without SPICE (i.e., with Simscape [10]), many of the spark-gap circuit models are constructed with a SPICE solver that could be integrated with an existing toolchain for electromagnetic field simulators. Our method will consist of building upon the recently verified model of Pouncey

and Lehr [6]. It has been originally implemented in LTSpice as a rather complex circuit with numerous behavioral sources. Our effort was to simplify the model and express it in a programming language rather than solely with electrical circuit elements. Essentially, the spark-gap model represents an arc channel as a nonlinear resistor in series with a nonlinear inductor. While the original model of a single spark-gap in LTSpice requires solving a matrix with 45 rows, our model in ACME.jl operates on matrices with no more than four rows. Of course, this is the result of implementing nontrivial functions with circuit elements. In general, the proposed and simplified model could handle a greater number of spark-gaps much more easily. However, in this paper we consider the field simulations coupled with circuits with only a single spark-gap.

The electrical circuit in Figure 1 represents an electrical arc between spark-gaps' electrodes. Both the  $R$  resistance and the  $L$  inductance depend on the radius of the arc channel for a given  $i$  current flowing after an electrical breakdown of the spark-gap. The radius of the  $r_{ch}$  channel can be calculated by the Braginskii equation [11]. It depends on the gas pressure, the time since the arc channel has been created and the magnitude of the current through the channel. The radius is a parameter for the formulas calculating the resistance and inductance of the arc channel. There are different models of the resistance value of an electrical arc. They were verified with measurements and compared in [12] with a reasonable agreement. In our work,  $R$  resistance is modeled with Vlastós equation [13]. The last nonlinear parameter of the discharge is the arc's inductance. Generally, the arc is treated as a straight wire of a  $r_{ch}$  radius and the  $d$  length (where  $d$  is the distance between spark-gap electrodes). Interestingly, the calculated inductance value alone sometimes resulted in a discharge that failed to cease as the current seemed to approach a significant value. In our model, an additional inductor has been connected in series with the spark-gap to lower the chance of creating an everlasting arc discharge. The inductor represents the inductance of the physical metal connectors of the spark-gap and its value is in the range of a few nanohenries.

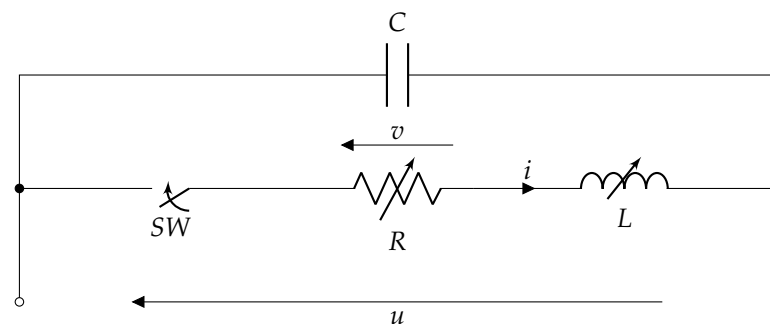


**Figure 1.** Equivalent circuit of a spark-gap consisting of nonlinear arc resistance  $R(i, t)$ , nonlinear arc inductance  $L(i, t)$ , spark-gap electrodes' capacitance  $C$ , and a switch representing the presence of an arc channel.

The SW switch in Figure 1 controls the presence of a conducting channel between the electrodes. Its state is controlled by the  $u$  voltage across the electrodes. Before the breakdown, there is no arc channel, and the switch is open, and the  $v$  voltage drop on the  $R$  resistor equals the applied voltage  $u$ . Lastly, the constant  $C$  capacitance represents the capacitance between the electrodes.

In this work, we have decided to implement the three elements SW,  $R$  and  $L$  as a single, nonlinear element. It has simplified the definition of the circuit, as the nonlinear state variables  $\mathbf{q}$  consist of four components:  $\mathbf{q} = \{v, i, \Phi, u\}$ , where  $v$  is the voltage on the  $R$  resistor,  $i$  current flows through the arc channel,  $\Phi$  is the magnetic field flux associated with the  $L$  inductor, and  $u$  is the voltage across the spark-gap.

Contrary to most switches implemented in SPICE simulators, the SW switch is executed as a conditional statement that instantaneously connects the nonlinear resistor and inductor, rather than a time-varying resistance. This approach is similar to the piecewise-

linear model implemented by [14], although the switched series connection of  $R$  and  $L$  is nonlinear. Left out of the diagram in Figure 1 are the voltage source representing the applied voltage  $u$  and the current probe for measuring  $i$ . The two elements are also incorporated into the matrix for the circuit model. In order to solve the nonlinear circuit, the resulting matrices were extracted from the ACME.j1 model and they were solved with our implementation of Newton's method. It has enabled us to easily integrate the circuit solver with our own tool for automatic differentiation (described in Section 3), although there are plans to add the support for that directly in ACME.j1.

The evolution of the internal state of a spark-gap element is controlled by the procedure depicted in Figure 2. This procedure is executed after the solution of the nonlinear *field* solution is found. To advance the spark-gap element in time by  $\Delta t$ , it is needed to check if the element is currently conducting (the channel is established) or not.

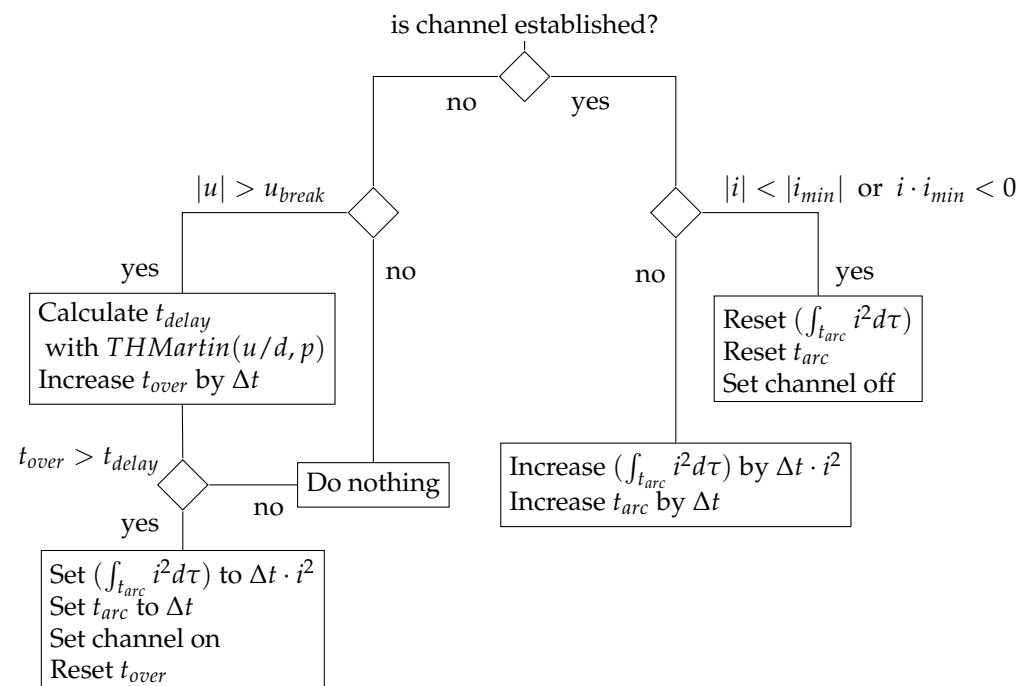


**Figure 2.** Diagram of the procedure for advancing the state of a realistic spark-gap.

If the element is not conducting, the  $i$  current is zero and the  $u$  voltage is tested for, exceeding the breakdown voltage  $u_{break}$ . The breakdown voltage can be calculated using a formula for static breakdown voltage in air from Bruce [15] or from Meek and Craggs [16]. Both formulas are valid in the case of uniform electric fields between electrodes up to about 10 atmospheres. Our implementation uses the formula from Meek and Craggs. Once the  $u$  voltage is higher than the static breakdown voltage, we start tracking the time  $t_{over}$  since the overvoltage has happened. After an overvoltage, the conducting channel takes some time to develop. The  $t_{delay}$  delay between the exceeding of the breakdown voltage and the formation of a spark can be approximated with a formula taken from [17]. As soon as the time since the overvoltage is longer than the delay, the spark-gap starts conducting the electric current. In the conducting state, two basic parameters are being tracked: the time since the channel has been established  $t_{arc}$ , and the cumulative time integral of the current squared ( $\int_{t_{arc}} i^2 d\tau$ ) during  $t_{arc}$ .

On the other hand, there is a minimal current that can sustain the channel. The test if the channel should be maintained is conducted in two ways. Firstly, we check if the current has not dropped below a certain threshold  $i_{min}$ . Secondly, we test if it has not changed its direction of flow as it would imply a zero-crossing. When there is not enough current to keep the channel conducting, both ( $\int_{t_{arc}} i^2 d\tau$ ) and  $t_{arc}$  are reset to zero and the channel is considered off.

### 3. Coupling Electromagnetic Field Simulators with Circuits Solvers

This paper describes an open-source implementation of a 2D time-domain Finite Element Method (TDFEM) solver using Whitney vector elements in the Julia programming language. The solver is based on the MATLAB codes accompanying the classical textbooks on computational electromagnetics by Davidson [18] and Rylander et al. [19].

The electromagnetic field solver for Blumlein pulse forming line (PFL) solves the following wave equation:

$$\frac{1}{\mu} \nabla \times \nabla \times \mathbf{E} + \varepsilon \frac{\partial^2}{\partial t^2} \mathbf{E} + \sigma \frac{\partial}{\partial t} \mathbf{E} = -\frac{\partial}{\partial t} \mathbf{J}_i, \quad (1)$$

where  $\mathbf{E}$  is an instantaneous electric field vector,  $\mu$ ,  $\varepsilon$  and  $\sigma$  are (respectively) the permeability, permittivity and conductivity of the medium filling PFL, while  $\mathbf{J}_i$  is an induced current density vector acting as an external source term. The material properties of the medium are constant in both time and space as presented in Figure 3a. The model represents a Blumlein pulse forming line which is composed of two parallel-plate transmission lines sharing one of their conductors (marked as  $\Gamma_B$ ). An important part of the model is the coupling between the circuit model and the field model, which is outlined in Figure 3b. The first transmission line is charged with a voltage source  $V_{in}$  connected through a high resistance  $R_s$  to  $\Gamma_1$ , while the second transmission line is terminated with a spark-gap, which is initially open (boundary  $\Gamma_2$ ). The outer conductors of two transmission lines are connected with  $R_L$  load (boundary  $\Gamma_3$ ). In fact, the load does not have to be a purely resistive element, it might be an arbitrary, passive one-port device (the case will be investigated in Section 4.2). When the device is charged to a sufficiently high voltage, the spark-gap will close and  $\Gamma_2$  will act as a conductor.

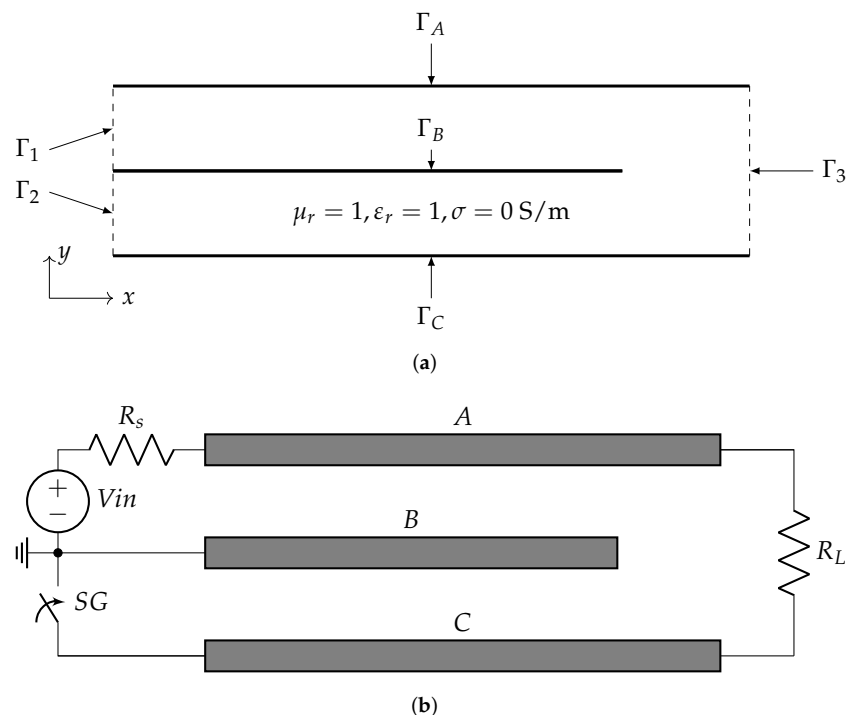


**Figure 3.** Model of a 2-D, parallel-plate Blumlein pulse forming line with an air dielectric. The solid black lines are perfect electric conductors (zero Dirichlet boundary condition), while the dashed lines are perfect magnetic conductors (default, natural Neumann boundary condition). (a) Model of the field simulation (not to scale). (b) Coupling between the circuit and field models (conductors A, B and C correspond to the boundaries  $\Gamma_A$ ,  $\Gamma_B$  and  $\Gamma_C$  from the field model).

From a weak formulation of (1) one can derive stiffness ( $\mathbf{S}$ , also called curl matrix) and mass matrices ( $\mathbf{T}$ ,  $\mathbf{R}$ ), given the assumption of homogeneous material parameters:

$$S_{ij} = \frac{1}{\mu_r} \iiint_V (\nabla \times \mathbf{N}_i) \cdot (\nabla \times \mathbf{N}_j) dV \quad (2)$$

$$T_{ij} = \mu_0 \cdot \varepsilon \iiint_V \mathbf{N}_i \cdot \mathbf{N}_j dV \quad (3)$$

$$R_{ij} = \mu_0 \cdot \sigma \iiint_V \mathbf{N}_i \cdot \mathbf{N}_j dV. \quad (4)$$

This leads to a well-known second-order partial differential equation which has to also be discretized in time:

$$\mathbf{T} \cdot \frac{\partial^2 \mathbf{e}}{\partial t^2} + \mathbf{R} \cdot \frac{\partial \mathbf{e}}{\partial t} + \mathbf{S} \cdot \mathbf{e} + g(\mathbf{e}) = 0, \quad (5)$$

where  $\mathbf{e}$  is a vector of coefficients of an electric field approximation on a finite element mesh, and  $g(\mathbf{e})$  is a nonlinear source term that will be used for circuit-field coupling. The FEM solver uses a common Newmark- $\beta$  (with  $\beta = 1/4$ ) time discretization scheme on a two-dimensional, Cartesian, structured grid (although triangular Whitney elements are also supported). The Whitney vector elements have been selected despite their low order, because of their simple coupling with linear [20] and nonlinear electrical circuits [21] described by Feliziani and Maradei.

The electric field  $\mathbf{E}$  is expanded using vector basis functions  $\mathbf{N}_i$  as:

$$\mathbf{E} = \sum_{i=1}^N e_i \mathbf{N}_i, \quad (6)$$

where  $N$  is the total number of edges in the mesh,  $\mathbf{N}_i$  is the vector basis function corresponding to the  $i$ -th edge, and  $e_i$  is the coefficient of the expansion. We find the coefficient vector  $\mathbf{e} = [e_1, e_2, \dots, e_N]^T$  by solving the system of nonlinear equations:

$$\mathbf{F} = \mathbf{A} \cdot \mathbf{e}^n - \mathbf{b} + g(\mathbf{e}^n) = 0, \quad (7)$$

where the matrix  $\mathbf{A}$  and the vector  $\mathbf{b}$  are constructed using matrices  $\mathbf{S}$ ,  $\mathbf{T}$ ,  $\mathbf{R}$  and the known solutions from two, previous timesteps  $\mathbf{e}^{n-1}$ ,  $\mathbf{e}^{n-2}$ :

$$\mathbf{A} = \frac{1}{\Delta t^2} \mathbf{T} + \frac{1}{4} \mathbf{S} \quad (8)$$

$$\mathbf{b} = \frac{2}{\Delta t^2} \mathbf{T} \cdot \mathbf{e}^{n-1} - \frac{1}{2} \mathbf{S} \cdot \mathbf{e}^{n-1} \quad (9)$$

$$- \frac{1}{\Delta t^2} \mathbf{T} \cdot \mathbf{e}^{n-2} - \frac{1}{4} \mathbf{S} \cdot \mathbf{e}^{n-2} - \frac{1}{2\Delta t} \mathbf{R} \cdot \mathbf{e}^{n-2} \quad (10)$$

$$g(\mathbf{e}) = \frac{1}{2\Delta t} \cdot \mu_0 \cdot l^2 \cdot \mathbf{j}^n - \frac{1}{2\Delta t} \cdot \mu_0 \cdot l^2 \cdot \mathbf{j}^{n-2} \quad (11)$$

$$G_{ii} = \partial g_i / \partial e_i = \frac{1}{2\Delta t} \cdot \mu_0 \cdot l^2 \cdot \partial j_i / \partial e_i, \quad (12)$$

where  $\mathbf{j}^n = [j_1(\mathbf{e}), j_2(\mathbf{e}), \dots, j_N(\mathbf{e})]^T$  is a vector of currents flowing through each mesh edge for a given excitation voltage.

An important distinction from the work of Feliziani and Maradei is the temporal discretization of the connected electrical circuits. Their work [21] describes a way of connecting resistors, capacitors and inductors to edges of an FEM mesh by adding their values directly to  $\mathbf{R}$ ,  $\mathbf{T}$  and  $\mathbf{S}$  matrices (respectively). This way, the circuit elements are also discretized using the Newmark- $\beta$  scheme. In our solution, we use the trapezoidal integration rule used by default by ACME.jl [7] to allow uniform treatment of arbitrary circuits.

As the source term  $g(\mathbf{e}^n)$  depends on the *yet unknown* edge voltages, the Newton method has been used for finding the solution of the nonlinear problem. The control

flow of the main loop of the simulator is presented in Figure 4. We distinguish the final solution  $\mathbf{e}$  at each timestep from an intermediate result during the Newton iterative method  $\hat{\mathbf{e}}$ . The intermediate result is used for calculating the currents flowing through circuits' terminals. The iterative procedure stops as soon as a norm of  $\Delta\hat{\mathbf{e}}$  is lower than  $10^{-12}$  or after 10 iterations. It is worth noting that, internally, the circuit might also need to solve another nonlinear problem  $f(\mathbf{q})$ . From the point of view of a circuit model, the voltages  $\hat{\mathbf{e}}^n$  are considered *fixed*.

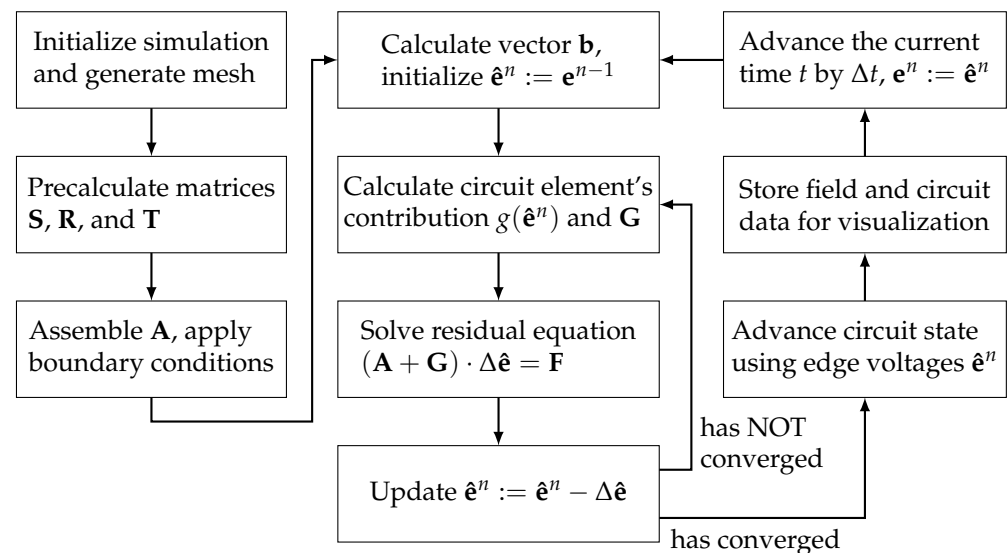


**Figure 4.** Diagram of the control flow in the field simulator. The inner workings of the circuit solver are left for brevity.

#### Automatic Differentiation

Calculations of both  $\partial f / \partial q_i$  and  $\partial g_i / \partial e_i$  are carried out using the automatic differentiation method. The method is a technique for evaluating partial derivatives using the chain rule of differentiation. There are three main approaches to automatic differentiation, i.e., forward accumulation, reverse accumulation and source-to-source differentiation. They differ by way of the computational overhead of evaluating the derivatives. However, they all calculate the result with machine precision [22]. Reverse accumulation (and to a lesser extent source-to-source differentiation) is a vital part of modern deep neural networks, where derivatives used for backward propagation of errors are calculated using an automatic differentiation method.

Our simulation code uses our own implementation of hyperdual [23,24] numbers  $h = a + \epsilon_u b + \epsilon_i c$ . The two dual units  $\epsilon_u$  and  $\epsilon_i$  correspond respectively to the derivative of an expression for the edge voltage  $u$  and for the current  $i$  through that edge. This way, we do not need to use any analytical derivative functions.

#### 4. Numerical Experiments

To assess the applicability of the circuit spark-gap model, two numerical experiments have been carried out. All of them share the same 2D field model, which describes a parallel-plate Blumlein pulse forming line. The computational domain has the length  $L_x = 2$  m and the height  $L_y = 0.08$  m. The outer conductors  $A$  and  $C$  have the length  $L_x$  and are defined on the top and bottom boundaries of the domain, while the middle conductor has a shorter length  $L_B = 1.9$  m. The distance between conductors  $A - B$  and  $B - C$  is the same and equals half of the computational domain's height. Air has been chosen as the dielectric for the setup with  $\epsilon_r = 1$ ,  $\mu_r = 1$  and  $\sigma = 0$  S/m. As a result, the characteristic impedance of each of the PFL's transmission lines is  $Z_0 \approx 13.2 \Omega$ , so the matched load should be  $R_L = 2Z_0 = 26.4 \Omega$ .

In order to assure reasonable accuracy of the electromagnetic waves propagating in the structure, the domain is discretized with a mesh  $100 \times 4$  of rectangular Whitney elements. All the experiments assume a fixed timestep  $\Delta t = 50$  ps which seems to allow resolving the fine details of the propagating pulses. The circuit simulations are also solved with the same timestep. In all of the simulations, the spark-gap is operating in the atmospheric air, at standard temperature and pressure. The distance between the electrodes is assumed to be  $d = 1$  mm. The parasitic parameters of the spark-gap are the following:  $C_{sg} = 0.3$  pF,  $L_{sg} = 3$  nH. The conducting channel is assumed to vanish when the current through the spark-gap drops below  $|i_{min}| = 10$   $\mu$ A.

#### 4.1. Matched, Resistive Load

The first test verifies the basic mode of operation of Blumlein PFL. In theory, after both (identical) transmission lines in a PFL are charged to a high voltage  $V$ , shorting one of two of the transmission lines would initiate a wave of a collapsing voltage. The wave should travel up to the load connecting the outer conductors of both lines. If the load has twice the value of the characteristic impedance of the lines, the wave reflected from the load and the wave transmitted should have the same magnitudes but opposite phases. Furthermore, if the other transmission line has an open end, then at the load we could expect a single, rectangular pulse of the amplitude close to the voltage  $V$ .

In this experiment, we are after the effects of the wave phenomena and the spark-gap's parameters on the operation of Blumlein PFL. The load connected between the outer conductors of the transmission lines is an ideal resistor with the resistance  $R_L$ . As can be seen in Figure 5, charging the transmission lines through a resistor  $R_s = 3$  k $\Omega$  takes approximately 1.59  $\mu$ s and after that the first pulse is generated. Transit time of the voltage pulse through the two  $L_B = 1.8$  m lines is approximately  $\tau = L/c \approx 6$  ns. The pulse width is twice the transit time which seems to be confirmed, except for the tail after the main pulse.

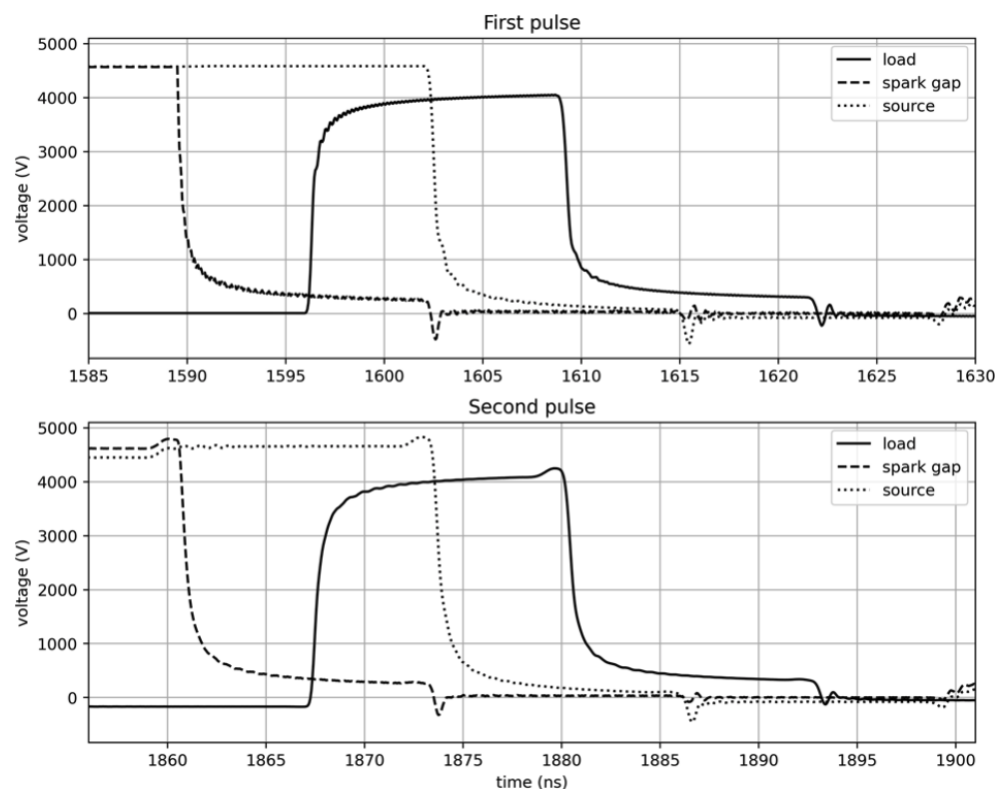


**Figure 5.** Voltages across the matched load, the spark-gap (realistic model) and the high voltage DC power source.

After the first pulse is delivered to the load, the spark-gap opens again approximately  $4\tau = 25$  ns after the pulse has started. As the high voltage source is still connected, the Blumlein line is being charged the second time, and we observe the second pulse. Because the PFL is not discharged completely, the charging before the second pulse is faster and the resulting voltage waveform is slightly different from the first one. It is due to some residual reflected waves traveling inside the transmission lines; however, the main parameters of the pulse are similar.

Computer simulation helps with inspecting the influence of the different parameters of our PFL model. For that, a simplified, baseline simulation was prepared with a time-varying resistor  $R_{sg}(t)$  in parallel with a  $C_{sg}$  capacitor representing a spark-gap. The smooth transition between the high and low resistance value changes as a sigmoid function:  $R_{sg}(t) = R_{closed} + R_{open} - R_{open} / (1.0 + e^{-\alpha t})$ , where  $t$  is time in nanoseconds since the resistance starts decreasing,  $R_{closed} = 1.5 \Omega$  is the resistance after the switch is fully closed,  $R_{open} = 10^{12}$  is the resistance when the spark-gap is not conducting, and  $\alpha = 10$  controls how fast the switch closes. The value of  $\alpha$  has been chosen arbitrarily, so that the switch closes in approximately 2 ns.

The voltage waveforms presented in Figure 6 suggest that the tail of the primary pulse results from a non-zero resistance of the switch after closing. The parameter  $R_{closed}$  was chosen to match the minimal resistance of the arc channel in Figure 5.

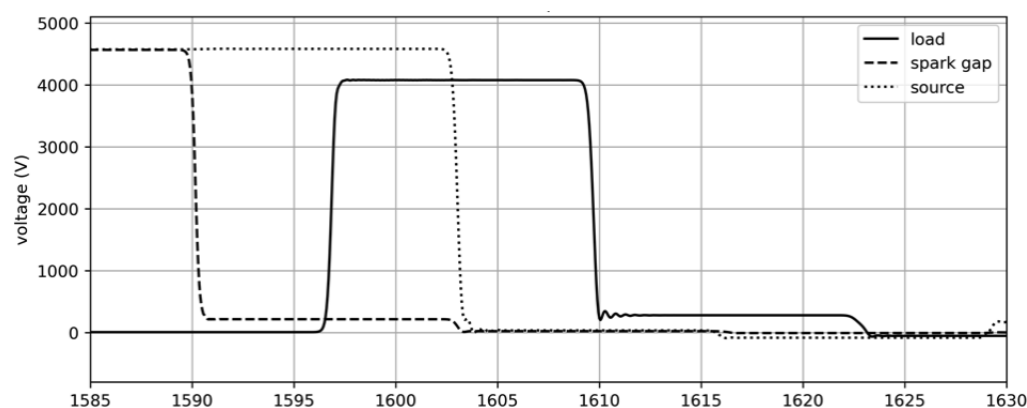


**Figure 6.** Voltages across the matched load, the spark-gap (a time-varying resistor) and the high voltage DC power source.

Other useful diagnostics are the plots of the time-varying resistance  $R(t)$  and inductance  $L(t)$  of the arc channel presented in Figure 7. It is noticeable that the parameters are slightly different for each pulse, which is mostly visible in the first 2–3 ns of the discharge. The plot of resistance is in logarithmic scale due to the rapid change of its value. It is important that the rate of the change determines the rise time of the pulse delivered to the load and it is not assumed in the circuit model, but rather it depends on the evolution of the spark channel due to the current flowing through the channel. On the other hand, inductance  $L$  is presented in linear scale, and most of the time through the discharge it has a value of around 5 nH. That would suggest that, in this case, using a constant value of  $L$  seems justified.

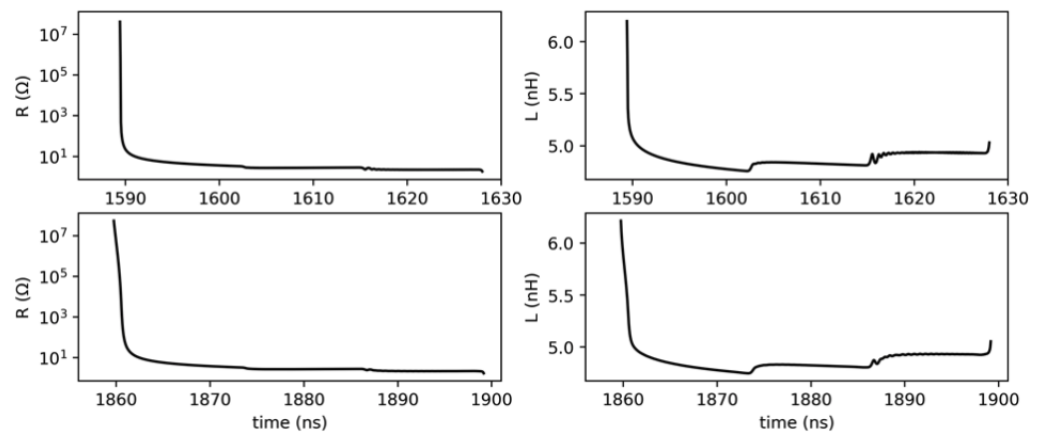


**Figure 7.** The nonlinear resistance (logarithmic scale) and inductance (linear scale) values of the arch channel during the pulse time depicted in Figure 5.

#### 4.2. Equivalent Circuit of a Dipole Antenna

Many applications of Blumlein PFL use an antenna connected as a load, which could be used for radiating the pulses as electromagnetic waves. To simplify the analysis of the PFL loaded with a radiating element, the antenna has been modeled as an equivalent circuit that represents the frequency characteristic of a real dipole antenna. A three-element equivalent circuit was adapted from [25], which describes a dipole antenna of a total length  $2h = 1.8$  m and radius  $a = 2.64$  mm. The parameters of the equivalent circuit are presented in Figure 8. The particular antenna is expected to behave poorly as the resonant frequency and input impedance are not matched to the pulse generator. However, it allows us to assess the overall performance of a more complex system. It is important to note that, as the dipole antenna has a gap between its two arms, a shunt connection has to be added in their form of a series connection of resistance  $R_{shunt}$  and inductance  $L_{shunt}$ . During the discharge, the shunt connection should be seen as a high impedance circuit for a fast rising pulse.

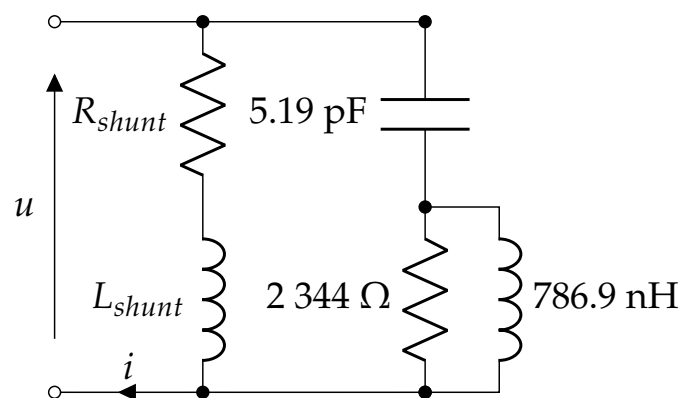


**Figure 8.** Equivalent circuit representing a dipole antenna. Shunt resistance and inductance are (respectively)  $100 \Omega$  and  $800 \mu\text{H}$ .

Voltage waveforms registered at the load (antenna) and at the spark-gap prove the existence of multiple reflections in Figure 9, both during the charging phase and also during the time that the spark-gap switch is conducting.

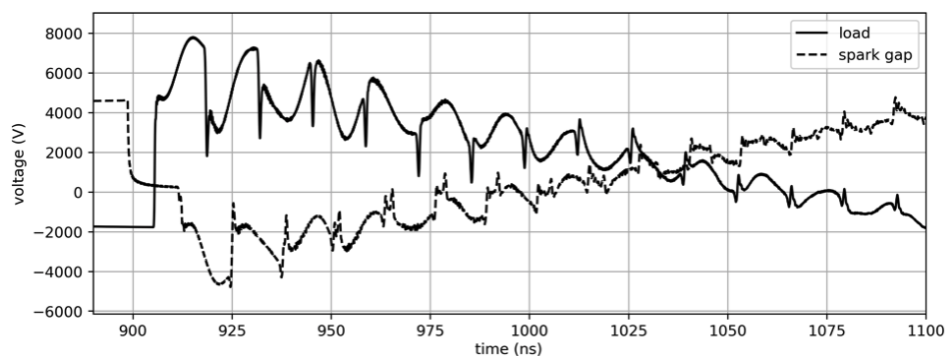


**Figure 9.** Voltage waveforms on the antenna terminals (load) and the spark-gap.

## 5. Results

The two experiments have proved that the coupled field-circuit simulation is performing well in modeling the Blumlein transmission line.

Comparing results for the realistic spark-gap model (in Figure 5) with a simple model (in Figure 6), it can be seen that the general waveform resembles a rectangular pulse, while the simpler model fails to capture distortions of the pulse by the realistic spark-gap. As the parasitic inductance and capacitance are present in the real switching devices it is too optimistic to assume an ideal rectangular pulse generated after shorting the spark-gap. In the simple model, the time at which the switch changes its state has to be precisely defined. This means that one has to know how many times (and when) the switch will be in closing and opening. This is hard to predict as it depends not only on the spark-gap but also on the load, as the electromagnetic wave reflected from the load after the first pulse might increase the voltage on the spark-gap above a threshold of static voltage breakdown. The first numerical experiment also allows the inspection of the time-varying inductance and the resistance of the realistic spark-gap model (in Figure 7). It is crucial that the parameters are dynamic and depend on general parameters of the spark-gap, i.e., electrode distance, gas pressure. On the basis of their value, one might even consider making them constant for a simplification (if needed).

The second numerical experiment used an equivalent circuit description of a dipole antenna as an example of a more complex load than a matched resistance. Of course, the antenna is not designed/matched to the PFL and behaves poorly, resulting in severe reflections of the propagating pulse from the load. Designing a pulse propagating antenna matched to the PFL is a demanding task, which is outside the scope of this research paper. To correctly represent the transmission line, a more sophisticated electromagnetic field solver had to be used (i.e., supporting 3D finite elements or an axial symmetry of the 2D domain). Figure 9 only shows the first voltage pulse, but after the breakdown the voltage across the spark-gap increases. This leads to another discharge. If one would prescribe the times at which a simpler spark-gap model switches its state, we would see a waveform similar to the one in Figure 9 (we have omitted that result for brevity). The point in this experiment is that while the waveform might be similar, it is hard to correctly determine all the parameters that one has to know (i.e., times of switching the spark-gap). In this case, a model with fewer parameters is preferable.

One of the main advantages of the circuit model is that, given few physical parameters (i.e., spark-gap's capacitance, inductance of the connectors, distance between the electrodes, pressure of the insulating gas), the model captures the basic characteristics of the high voltage switch, e.g., the rise time of the voltage pulse. At the same time, the field model allows an assessment of the interaction of the electromagnetic wave propagating with transmission lines that were not perfectly terminated. Both models are moderately computationally intensive. Each simulation required solving the electric field and circuit currents at 40,000 timesteps, which took less than 5 min. on an 8-core Apple M1 processor with 8 GB of RAM.

## 6. Discussion

Having a spark-gap model that can be integrated with a full-wave simulation is a useful tool for designing more efficient high voltage pulse generators. The presented computer model still relies on few assumptions. We assume that:

- We know the parameters of the spark-gap: the gas mixture, the gas pressure, the inductance, and capacitance of the electrodes and connected wiring;
- The spark-gap can be represented as a circuit of lumped elements, i.e., electromagnetic waves within the spark-gap are not represented;
- The field simulation is represented in a 2D Cartesian coordinate system: only parallel plate transmission lines of an infinite width (in z-direction) can be analysed;
- The relative permittivity and permeability have to be time-invariant and uniform over the computational domain.

Currently, one could use more than a single spark-gap, but the interaction between them is limited, and effects such as the pre-ionization of adjacent spark-gaps is not yet possible. However, despite the presented assumptions and limitations, the implemented circuit model allows us to capture the interaction of a spark-gap circuit with both simple (e.g., resistors) and complex (e.g., an equivalent circuit representing a dipole antenna) devices. To recreate the interaction using a simpler spark-gap model, one has to precisely prescribe the switching times and the parameters of the time-varying resistance of such a switch. There is still a need for a more detailed model of spark-gaps that will eliminate even more assumptions, but it will surely come with the cost of increased computational time and resources. At this state, the field solver supports only 2D simulations in the Cartesian coordinate system. In order to simulate devices such as switched wave oscillators or coaxial Blumlein transmission lines, a 2D simulation in a cylindrical coordinate system would be interesting. This will be pursued in our future research.

**Author Contributions:** Conceptualization, W.Ł. and B.C.; methodology, B.C.; software, B.C. and W.Ł.; validation, B.C. and W.Ł.; writing—original draft preparation, B.C. and W.Ł.; writing—review and editing, W.Ł. and B.C.; visualization, B.C. All authors have read and agreed to the published version of the manuscript.

**Funding:** This research received no external funding.

**Institutional Review Board Statement:** Not applicable.

**Informed Consent Statement:** Not applicable.

**Data Availability Statement:** The data presented in this study are openly available in a public repository <https://github.com/bchaber/fala> (accessed on 27 February 2022).

**Acknowledgments:** The authors would like to express their gratitude to Jan Sroka, Jacek Starzyński and the reviewers for their thoughtful and valuable comments on the first version of the paper.

**Conflicts of Interest:** The authors declare no conflict of interest.

## Abbreviations

The following abbreviations are used in this manuscript:

FEM	Finite Element Method
SPICE	Simulation Program with Integrated Circuits Emphasis
PFL	Pulse Forming Line
RAM	Random Access Memory

## References

1. Basso, C. Spice Model Simulates Spark-Gap Arrestor. *EDN Mag.* **1977**, 3–5.
2. Pouncey, J.C.; Lehr, J.M. A Spark-gap Model for LTSpice and Similar Circuit Simulation Software. In Proceedings of the 2015 IEEE Pulsed Power Conference (PPC), Austin, TX, USA, 31 May–4 June 2015. [[CrossRef](#)]

3. Benoît, M.; Raymond, P.; Wey, J. New model for ultracompact coaxial Marx pulse generator simulations. *Rev. Sci. Instrum.* **2006**, *77*, 043505. [[CrossRef](#)]
4. Worts, E.; Kovaleski, S.D. Theoretical Investigation of a UV Laser Triggered Spark-gap. In Proceedings of the 2005 IEEE Pulsed Power Conference (PPC), Austin, TX, USA, 31 May–4 June 2015. [[CrossRef](#)]
5. Achour, Y.; Starzyński, J.; Łasica, A. Compact nanosecond pulse generator based on IGBT and spark-gap cooperation. *Bull. Pol. Acad. Sci. Tech. Sci.* **2020**, *68*, 377–388. [[CrossRef](#)]
6. Pouncey, J.C.; Lehr, J.M. A Parametric SPICE Model for the Simulation of Spark-gap Switches. *Rev. Sci. Instrum.* **2020**, *91*, 034704. [[CrossRef](#)] [[PubMed](#)]
7. Holters, M.; Zölzer, U. A generalized method for the derivation of non-linear state-space models from circuit schematics. In Proceedings of the 2015 23rd European Signal Processing Conference (EUSIPCO), Nice, France, 31 August–4 September 2015; pp. 1073–1077. [[CrossRef](#)]
8. Holters, M. *HSU-ANT/ACME.jl+ (v0.9.5)*; Zenodo: Geneva, Switzerland, 2021. [[CrossRef](#)]
9. Bezanson, J.; Edelman, A.; Karpinski, S.; Shah, V.B. Julia: A Fresh Approach to Numerical Computing. *SIAM Rev.* **2017**, *59*, 65–98. [[CrossRef](#)]
10. Achour, Y.; Starzyński, J.; Łasica, A. New embedded nanosecond pulse generator based on spark gap and IGBT. In Proceedings of the 2017 IEEE 21st International Conference on Pulsed Power (PPC), Piscataway, NJ, USA, 18–22 June 2017; pp. 1–4. [[CrossRef](#)]
11. Braginskii, S.I. Theory of the Development of a spark channel. *Sov. Phys. JETP* **1958**, *34*, 1068–1074.
12. Santamaria, F.; Roman, F. Experimental Study of a Submillimeter Spark-Gap. *IEEE Trans. Plasma Sci.* **2013**, *41*, 985–992. [[CrossRef](#)]
13. Vlastós, A.E. The Resistance of Sparks. *J. Appl. Phys.* **1972**, *43*, 1987–1989. [[CrossRef](#)]
14. Allmeling, J.H.; Hammer, W.P. PLECS—Piece-wise linear electrical circuit simulation for Simulink. In Proceedings of the IEEE 1999 International Conference on Power Electronics and Drive Systems, PEDS'99 (Cat. No. 99TH8475), Hong Kong, China, 27–29 July 1999; Volume 1, pp. 355–360. [[CrossRef](#)]
15. Bruce, F.M. Calibration of uniform-field spark-gaps for high-voltage measurement at power frequencies. *J. Inst. Electr. Eng.-Part II Power Eng.* **1947**, *94*, 138–149.
16. Meek, J.M.; Craggs, J.D. *Electrical Breakdown of Gases*; Wiley: Hoboken, NJ, USA, 1978.
17. Martin, T.H. An empirical Formula for Gas Switch Breakdown Delay. In Proceedings of the Pulsed Power Conference, Monterey, CA, USA, 11–14 June 1989; pp. 73–79.
18. Davidson, D.B. *Computational Electromagnetics for RF and Microwave Engineering*, 2nd ed.; Cambridge University Press: New York, NY, USA, 2010; pp. 496–497. [[CrossRef](#)]
19. Rylander, T.; Ingelström, P.; Bondeson, A. *Computational Electromagnetics*; Springer: New York, NY, USA, 2013; pp. 117–127. [[CrossRef](#)]
20. Feliziani, M. Modeling of Electromagnetic Fields and Electrical Circuits with Lumped and Distributed Elements by the WETD Method. *IEEE Trans. Magn.* **1999**, *35*, 1666–1669. [[CrossRef](#)]
21. Feliziani, M.; Maradei, F. Circuit-Oriented FEM: Solution of Circuit-Field Coupled Problems by Circuit Equations. *IEEE Trans. Magn.* **2002**, *38*, 965–968. [[CrossRef](#)]
22. Kochenderfer, M.J.; Wheeler, T.A. *Algorithms for Optimization*; MIT Press: Cambridge, MA, USA, 2019; pp. 25–32. ISBN 9780262039420.
23. Khan, K.A.; Barton, P.I. A vector forward mode of automatic differentiation for generalized derivative evaluation. *Optim. Methods Softw.* **2015**, *30*, 1185–1212. [[CrossRef](#)]
24. Revels, J.; Lubin, M.; Papamarkou, T. Forward-Mode Automatic Differentiation in Julia. *arXiv* **2016**, arXiv:1607.07892.
25. Tang, T.G.; Tieng, Q.M.; Gunn, M.W. Equivalent Circuit of a Dipole Antenna Using Frequency-Independent Lumped Elements. *IEEE Trans. Antennas Propag.* **1993**, *41*, 1625–1632. [[CrossRef](#)]